13 Surface Physics

M. Hengsberger, L. Castiglioni, C. Monney, A. Hemmi, Z. Novotny, R. Totani, C. Bernard, A. Epprecht, L. Grad, P. Kliuiev, A. Kostanyan, A. Schuler, K. Waltar, W.-D. Zabka, J. Chen, F. Cossalter, M. Hotz, P. Kretz, H. Nussbaumer, D. Schachtler, B. Tobler, B. Salzmann, P. Dona, T. Kälin, T. Greber, and J. Osterwalder

Our laboratory is equipped for the investigation of surface and interface phenomena at the atomic level, for the preparation and characterization of clean single-crystalline surfaces, metal and molecular monolayer films, as well as sp^2-bonded single layers on surfaces that we exfoliate from metals with wet transfer methods. In addition, we are part of a user consortium of the soft x-ray beamline *PEARL (PhotoEmission and Atomic Resolution Laboratory)* at the Swiss Light Source. Our group has built and commissioned a compact and mobile angle-resolved photoemission (ARPES) instrument, while a second ARPES spectrometer has been successfully fitted with a high-harmonic gas jet source for producing short VUV light pulses.

The research carried out during the report period can be grouped into four topics:

- 2D materials
  Monolayer hexagonal boron nitride (*h*-BN) and graphene are grown by chemical vapor deposition (CVD) on metal surfaces. The present efforts focus on the delamination of theses single-layer materials from their growth substrate. For this purpose we develop wet transfer protocols that allow transfer of large-area hexagonal boron nitride onto arbitrary substrates. This project is pursued within the European FET Flagship Graphene (see Section 13.1).

- Adsorbed molecular catalysts and photosensitizers
  Within the University Research Priority Program *Light to Chemical Energy Conversion* (LightChEC) we develop and characterize model electrode surfaces for solar water splitting. Studied systems include monolayers of catalyst molecules on oxide semiconductor surfaces and self-assembled monolayers of photosensitizer molecules on ultrathin oxide films. Section 13.2 describes the preparation of ultrathin crystalline alumina films and the *in situ* adsorption of organometallic rhenium complexes with covalent linkers from solution in a specifically designed satellite chamber of our electron spectrometer.

- Ultrafast processes at surfaces
  Within the NCCR *Molecular Ultrafast Science and Technology* (MUST) the group investigates dynamical processes at surfaces on the pico- and femtosecond time scale by means of pump-probe photoemission experiments. This year we report on a polarization-sensitive terahertz pulse reconstruction scheme. It may be obtained from momentum-resolved photoelectron streaking data and recovers the field amplitudes and phase in THz laser pulses (see Section 13.3). This work is relevant for experiments at free electron lasers that use THz pump and x-ray probe pulses.

- Spin shuttles
  Fullerenes with magnetic endohedral units (*spin shuttles*) like $HoSc_2N@C_{80}$ are investigated in view of their magnetic properties. In this context we demonstrated that the molecular conformation may be changed with an external magnetic field [1] and that these nanometer sized molecules realize the smallest compass. This project bases on a collaboration with the IFW Dresden where the molecules are produced and purified.

We like to highlight the award of a Semesterpreis to Björn Salzmann for his Bachelor thesis *Doping Graphene on SiO_2 using X-rays*. Furthermore we organized within the Sino Swiss Science and Technology (SSSTC) cooperation a small international *workshop on endohedral single molecule magnets* in Castasegna.

In the following, three highlights of last year's research are presented in more detail.

[1] A. Kostanyan *et al.*,
Phys. Rev. Lett. **119**, 237202 (2017).

13.1 Centimeter-Sized Single-Orientation Hexagonal Boron Nitride

In collaboration with: Huanyao Cun, Ke Liu, Duncan T. L. Alexander, Aleksandra Radenovic, École Polytechnique Fédérale de Lausanne, Switzerland, Armin Kleibert, Swiss Light Source, Paul Scherrer Institut, Switzerland, Benjamin Probst, Department of Chemistry, Universität Zürich, Michael Weinl, Matthias Schreck, Institut für Physik, Universität Augsburg, Germany.

In this project we are producing single-layer material like graphene or hexagonal boron nitride (*h*-BN) on single-crystalline transition metal surfaces. The chemi-

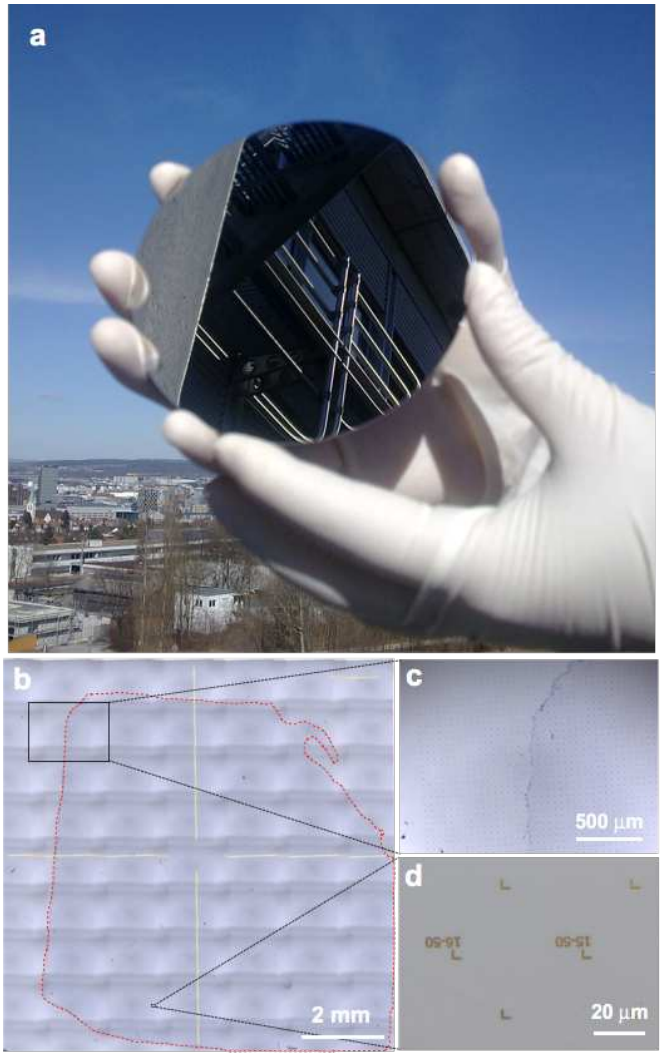

FIG. 13.1 – (a) Photograph of a four-inch wafer in Zürich air on which single layer *h*-BN may be grown. (b-d) Optical microscopy from single layer *h*-BN transferred on a 90 nm SiO_2/Si wafer. (b) 9.5 x 9.5 mm^2 where 64 individual frames are stitched together. The red line marks the boundary of the transferred *h*-BN. (c) Single frame from (b) containing the *h*-BN border. The single layer on the right side appears darker. (d) Zoom in where the gold markers that allow to find the same coordinates in different instruments are the only inhomogeneities. Data from [2].

cal vapor deposition growth method bears the advantage of scalability and substrate based functionalisation. Fig. 13.1(a) shows a four-inch wafer substrate with a single-crystalline metal film that is used in our lab for the production of single orientation *h*-BN on large areas. For applications in electronic devices, or as ultimately thin membranes, the material has to be transferred to insulating substrates or onto supporting grids. For *h*-BN, wet transfer methods that rely on electrochemical hydrogen-bubble production at the interface between the monolayer and the transition metal rhodium (111) surface yield flakes in the 20 µm size range. In a significant leap we succeeded to transfer centimeter sized single-layer *h*-BN onto arbitrary substrates [2]. Similar to the delamination of graphene from Ir(111) [3], the process involves an additional step prior to the H_2-bubbling, where the *h*-BN on Rh substrate is electrochemically treated in a tetraoctylammonium bromide (TOABr) solution in acetonitrile. After the TOA *h*-BN treatment transfer rates above 90% are obtained. Figures 13.1(b)-(d) show transferred centimeter sized single-layer, single-orientation *h*-BN on a 90 nm SiO_2/Si(001) wafer chip with micrometer sized gold markers that serve for navigation at the nanometer scale. The images are obtained with an optical microscope in air. The optical contrast of a single layer *h*-BN that may be used for identification of the transferred material on 90 nm SiO_2/Si is shown in Fig. 13.1(c). Although the centimeter sized *h*-BN does not (yet) meet the performance of the µm sized flakes that are exfoliated from *h*-BN single crystals [4], our material opens new perspectives for applications of monolayer-thick hexagonal boron nitride. It was demonstrated that it can protect germanium from oxidation at elevated temperatures, and that in functionalized form it can be used as an ion conducting membrane in a liquid [2], which was highlighted in Science [5].

[2] H.Y. Cun *et al.*, Nano Lett. **18**, 1205 (2018).

[3] L. Koefoed *et al.*, J. Phys. D: Appl. Phys. **48**, 115306 (2015).

[4] T. Taniguchi, and K. Watanabe, J. Cryst. Growth, **303**, 525 (2007).

[5] S. Vignieri and J. Smith, Science, **359**, 649 (2018).

13.2 Growth and functionalization of ultrathin crystalline alumina films

In collaboration with: Mathias Mosberger, Benjamin Probst and Roger Alberto, Chemistry Department, Universität Zürich (URPP LightChEC).

We investigated the growth of ultrathin crystalline alumina films and their functionalization with organometallic rhenium complexes. These are synthetically versatile photo- and redox active compounds and can be incorporated into efficient homogeneous photocatalytic systems [6].

Ultrathin alumina films grown by selective oxidation on NiAl(110) substrates are a prototypical example for ultrathin wide gap insulators with a minimum thickness of two atomic layers [7]. The structural changes in these crystalline films were studied systematically when the thickness is increased. The long-range order that does not

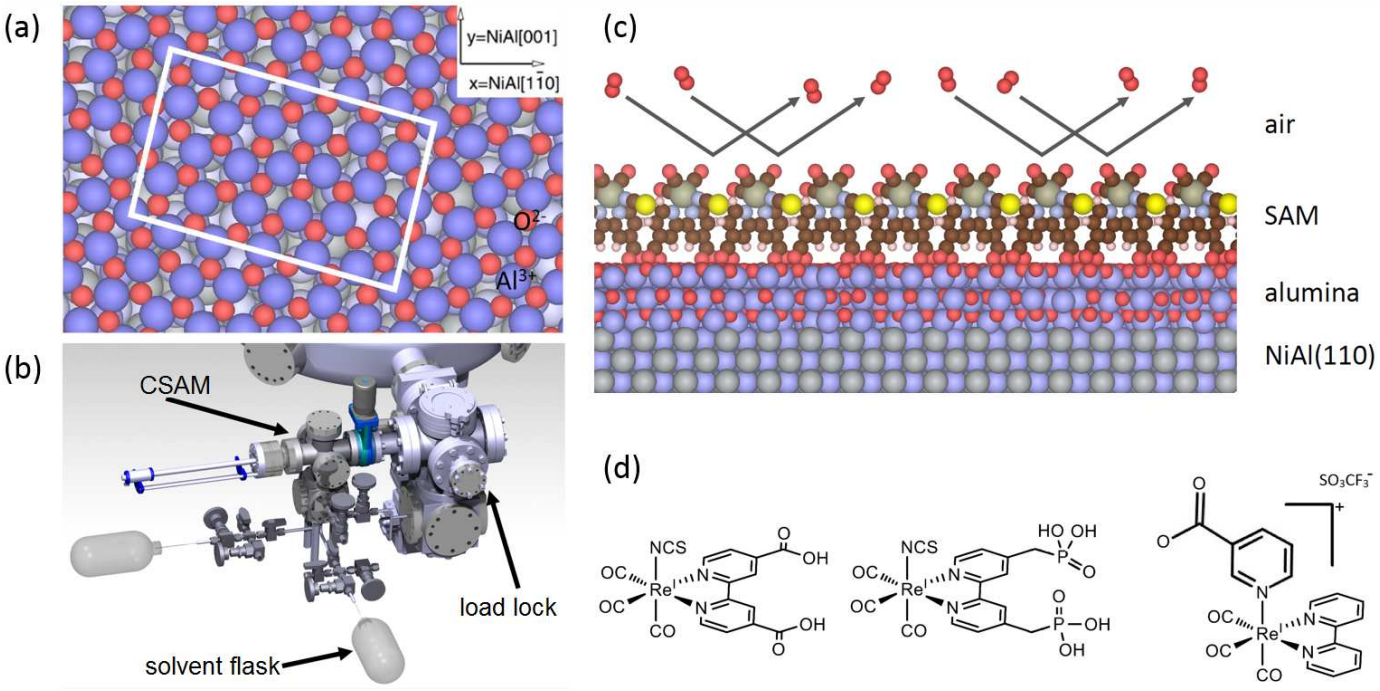

FIG. 13.2 – (a) Structure of a two-atomic-layers thick alumina film grown on NiAl(110) (unit cell marked in white, based on the model from Ref. [9]). (b) 3D rendering of the developed chamber (SAMcham) for self-assembled monolayers SAM deposition without exposing the samples to air. (c) Illustration of the produced metal-insulator-SAM heterostructure and the passivation effect. The SAM passivates the substrate in air. (d) Structure formulae of rhenium based organometallics with covalent linkers that were successfully attached to ultrathin alumina films.

relate to any bulk structure, is imposed by the crystallized interface, and is characterized by a rather large surface unit cell as shown in Fig. 13.2(a). This surface unit cell formed at the interface persists in thicker films. In contrast, the short-range ordering changes upon film growth and is attributed to the formation of subnanometer-sized $\gamma - Al_2O_3$-type nuclei inside the larger unit cell [8].

These ultrathin alumina films are prepared in ultra-high vacuum systems. The instability of these films under ambient conditions limits the possibilities of applications of these systems when the thickness of the insulating oxide film is crucial for device performance. Therefore, a chamber was developed and attached to our UHV system that allows to directly deposit organometallic rhenium complexes from solution with covalent linkers as illustrated in Fig. 13.2(b). Self-assembled monolayers (SAM) can thus be formed from a solution without sample exposure to air. The molecular layer acts as a capping layer, passivating the ultrathin oxide film against corrosion under ambient conditions (Fig. 13.2(c)). This method for molecule attachment was demonstrated to work for various photoactive organometallics (Fig. 13.2(d)), which allowed to compare their adsorption behavior and electronic level alignment to the substrate.

[6] B. Probst *et al.*, Inorg. Chem. **48**, 1836 (2009).

[7] Q.-H. Wu *et al.*, Int. Rev. Phys. Chem. **28**, 517 (2009).

[8] W.-D. Zabka *et al.*, Phys. Rev. B, **96**, 155420 (2017).

[9] G. Kresse *et al.*, Science, **308**, 1440 (2005).

13.3 Polarization-sensitive pulse reconstruction by momentum-resolved photoelectron streaking

In collaboration with: Johannes Haase (Laboratory for Catalysis and Sustainable Chemistry, Paul Scherrer Institute, Switzerland), Jeroen A. van Bokhoven (Department of Chemistry, ETH Zurich, Switzerland), Matteo Lucchini (Physics Department, Politechnico di Milano, Italy) (NCCR MUST).

Many pump-probe experiments nowadays aim at the investigation and manipulation of ultrafast dynamic processes at surfaces [10]. For instance, a THz pulse can interact with the dipole moment of adsorbed molecules and induce coherent atomic motion [11]. The structural dynamics of such motion is accessible via , e.g., x-ray photoelectron diffraction (XPD) [12]. A decisive experimental parameter in these types of experiments is the time-dependent strength and orientation of the electric field in close proximity to the surface under investigation. This effective electric field often results from the superposition of an incoming and reflected laser pulse and has a complex nature varying in space and time. In this work [13],

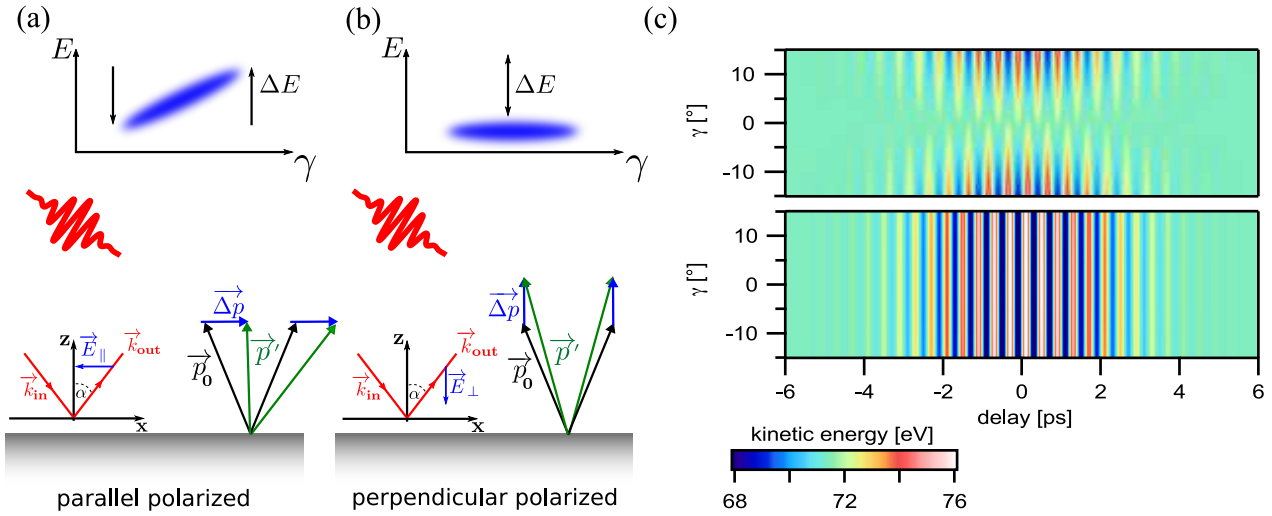

FIG. 13.3 – Schematic illustration of the effects of THz field components polarized parallel and perpendicular to the surface on the x-ray-emitted photoelectron momentum distribution (from [13]). (a) Effect of the electric field component parallel to the surface. The effective electric field due to superposition of incoming and reflected THz light with wavevectors $\vec{k}_{in}$ and $\vec{k}_{out}$ induces a momentum change $\vec{\Delta p}$ to the initial electron momentum $\vec{p}_0$ which results in a final momentum $\vec{p}\,'$. The effect on the detected electron distribution as measured in the two-dimensional electron analyzer is depicted at the top. γ is the detector angle and E the kinetic energy. (b) Same as in (a) but for the THz field component perpendicular to the surface. (c) COM maps of photoelectrons with an initial kinetic energy of 72 eV interacting with a Gaussian-shaped THz pulse with a peak amplitude of 10^7 V/m ($\lambda = 150$ µm, FWHM = 5 ps). The presented COM maps are shown for the case of a transparent substrate, i.e. with no reflection present. The anti-symmetric (top) and symmetric (bottom) energy shifts with respect to the normal emission direction $\gamma = 0°$ are hallmarks of the parallel and perpendicular field component.

we developed a pulse metrology to reconstruct the effective electric field components parallel and perpendicular to arbitrary metallic or dielectric surfaces by means of THz-field modified electron momentum distributions as measured in photoelectron spectroscopy experiments.

Photoelectrons are generated by a short x-ray pulse at a solid surface and undergo a momentum change due to interaction with a few-cycle THz pulse. The electron analyzer is capable of tracking changes in both, electron kinetic energy and angular distribution. Assuming a linearly polarized electric field, the effect of field components purely parallel and perpendicular to the surface is schematically shown in Fig. 13.3. Panel (a) elucidates the change to the detected electron distribution induced by a parallel field component. A parallel component leads to a lateral shift in the momentum distribution and hence to energy shifts that are roughly anti-symmetric to the normal emission direction. The perpendicular component in Fig. 13.3(b) causes a symmetric change in the momentum distribution and a symmetric energy offset relative to the interaction-free distribution. For each angular channel of the detector an energetic center of mass (COM) position can be determined that reflects the position of, for instance, an elastic photoemission line. THz-field induced changes in the electron distribution can then be followed in COM maps as shown in Fig. 13.3(c). These maps present the COM position of the electron distribution color-coded as a function of detector angle γ and relative delay between x-ray and THz pulse. The anti-symmetric energy modifications along the angle-dispersive axis due to the parallel field component Fig. 13.3(c, top), as well as the symmetric changes due to the perpendicular component Fig. 13.3 (c, bottom) are apparent. Our model uses the kinetic energy offset along the normal emission channel ($\gamma = 0°$) and the tilt angle of the COM distribution along the angle-dispersive axis as measures for the electron momentum added by the THz field which in turn can be related to the THz field components. We tested the validity of our model at different interfaces described by their optical constants. By using a Monte Carlo approach we were able to simulate artificial pump-probe experiments on a variety of substrates and with different optical parameters of the x-ray and THz pulse. We could validate our reconstruction approach by comparing the obtained field amplitudes to those calculated by Fresnel's equations and suggest suitable photoelectron energy regimes for optimal field reconstruction.

[10] J.L. LaRue *et al.*, Phys. Rev. Lett. **115**, 036103 (2015).

[11] S.S. Dilhon *et al.*, J. Phys. D: Appl. Phys. **50**, 043001 (2017).

[12] M. Greif *et al.*, Struct. Dyn. **2**, 035102, (2015).

[13] K. Waltar *et al.*, Opt. Express **26**, 8364-8374 (2018).